

Reciprocal skin effect and its realization in a topoelectrical circuit

Tobias Hofmann,¹ Tobias Helbig,¹ Frank Schindler,^{2,3} Nora Salgo,² Marta Brzezińska,^{4,2} Martin Greiter,¹ Tobias Kiessling,⁵ David Wolf,² Achim Vollhardt,² Anton Kabaši,⁶ Ching Hua Lee,^{7,8} Ante Bilušić,^{6,9} Ronny Thomale,¹ and Titus Neupert²

¹*Institute for Theoretical Physics and Astrophysics, University of Würzburg, Am Hubland, D-97074 Würzburg, Germany*

²*Department of Physics, University of Zurich, Winterthurerstrasse 190, 8057 Zurich, Switzerland*

³*Kavli Institute for Theoretical Physics, University of California, Santa Barbara, CA 93106, USA*

⁴*Department of Theoretical Physics, Faculty of Fundamental Problems of Technology,*

Wrocław University of Science and Technology, 50-370 Wrocław, Poland

⁵*Physikalisches Institut and Röntgen Research Center for Complex Material Systems, Universität Würzburg, D-97074 Würzburg, Germany*

⁶*Centre of Excellence STIM, University of Split, Poljička cesta 35, HR-21000 Split, Croatia*

⁷*Department of Physics, National University of Singapore, Singapore, 117542.*

⁸*Institute of High Performance Computing, A*STAR, Singapore, 138632.*

⁹*University of Split, Faculty of Science, Ruđera Boškovića 33, HR-21000 Split, Croatia*

(Dated: June 5, 2020)

A system is non-Hermitian when it exchanges energy with its environment and non-reciprocal when it behaves differently upon the interchange of input and response. Within the field of metamaterial research on synthetic topological matter, the skin effect describes the conspiracy of non-Hermiticity and non-reciprocity to yield extensive anomalous localization of all eigenmodes in a (quasi) one-dimensional geometry. Here, we introduce the reciprocal skin effect, which occurs in non-Hermitian but reciprocal systems in two or more dimensions: Eigenmodes with opposite longitudinal momentum exhibit opposite transverse anomalous localization. We experimentally demonstrate the reciprocal skin effect in a passive RLC circuit, suggesting convenient alternative implementations in optical, acoustic, mechanical, and related platforms. Skin mode localization brings forth potential applications in directional and polarization detectors for electromagnetic waves.

I. INTRODUCTION

First developed in the late 1920s by Felix Bloch and contemporaries [1], the electronic band theory of crystals has experienced an unprecedented revival of interest and sophistication through the theoretical and experimental discovery of topological matter [2–4]. Whereas band theory was previously employed in the context of infinite systems, the study of topological insulators [5, 6] and semimetals [7] has reshaped attention to the interplay of bulk and boundary degrees of freedom, culminating in the celebrated bulk-boundary correspondence [8, 9]. It allows for the prediction of universal boundary phenomena from bulk properties and relies on the fact that changing boundary conditions does not affect the bulk states at large. The predominant framework for topological crystal matter has been closed systems at zero temperature, whose band spectrum is obtained from a Hermitian Bloch Hamiltonian.

Recently, open systems that do not conserve energy or particle number have received significant attention. Within band theory, open systems are modeled by non-Hermitian Hamiltonians. The study of topological phases supported by such Hamiltonians yields qualitatively novel phenomena [10, 11], such as the occurrence of stable defective degeneracy points, so-called exceptional points [12, 13]. In two-dimensional systems [14], they are connected by bulk Fermi arcs [15]. Another exotic feature resolved through the band theory description of open systems is the non-Hermitian skin effect [16]: *all* of the eigenstates of a one-dimensional system can localize at one of its boundaries. The skin effect constitutes a breakdown of bulk-boundary correspondence, which is not found in closed systems [17–20].

The non-Hermitian skin effect has been discussed in one-

dimensional systems, and was initially assumed to necessitate a non-reciprocal Bloch Hamiltonian usually realized through asymmetric, direction-dependent hoppings. Reciprocal versions of the one-dimensional skin effect can be constructed by introducing additional degrees of freedom. Their protection against hybridization is realized by demanding additional symmetries such as mirror symmetry [21, 22]. In this work, we present a generalized skin effect in reciprocal systems, that is enabled by non-Hermiticity in dimensions higher than one. For simplicity, we constrain ourselves to two spatial dimensions. The basic idea is that, while a reciprocal model cannot localize all of its OBC eigenstates at just one boundary, it may still do so for states of a particular boundary momentum. Reciprocity then implies that the eigenstates at opposite momenta are localized at opposite boundaries.

The reciprocal skin effect dramatically expands the scenarios in which anomalous extensive skin mode localization [19] can be found in nature. As a paradigmatic experimental realization within a framework of high accessibility and tunability, we implement the reciprocal skin effect within a topoelectrical circuit setup. Similar to many other classical platforms of synthetic topological matter, this roots in the insight that Berry phase phenomena [23, 24] directly carry over to classical physics [25], since they do not concern phase space, but parameter space. The realization of topological phases in photonic [26], mechanical [27, 28] and electrical systems [29–38] explicates this connection between topological aspects of quantum and classical systems. The non-Hermitian band theory of open quantum systems can similarly be mirrored by descriptions of classical systems that involve gain and loss. Electric circuits whose circuit Laplacian [32] is modeled in analogy to a quantum Bloch Hamiltonian are particularly suited for this: loss and gain can be directly implemented by resistors

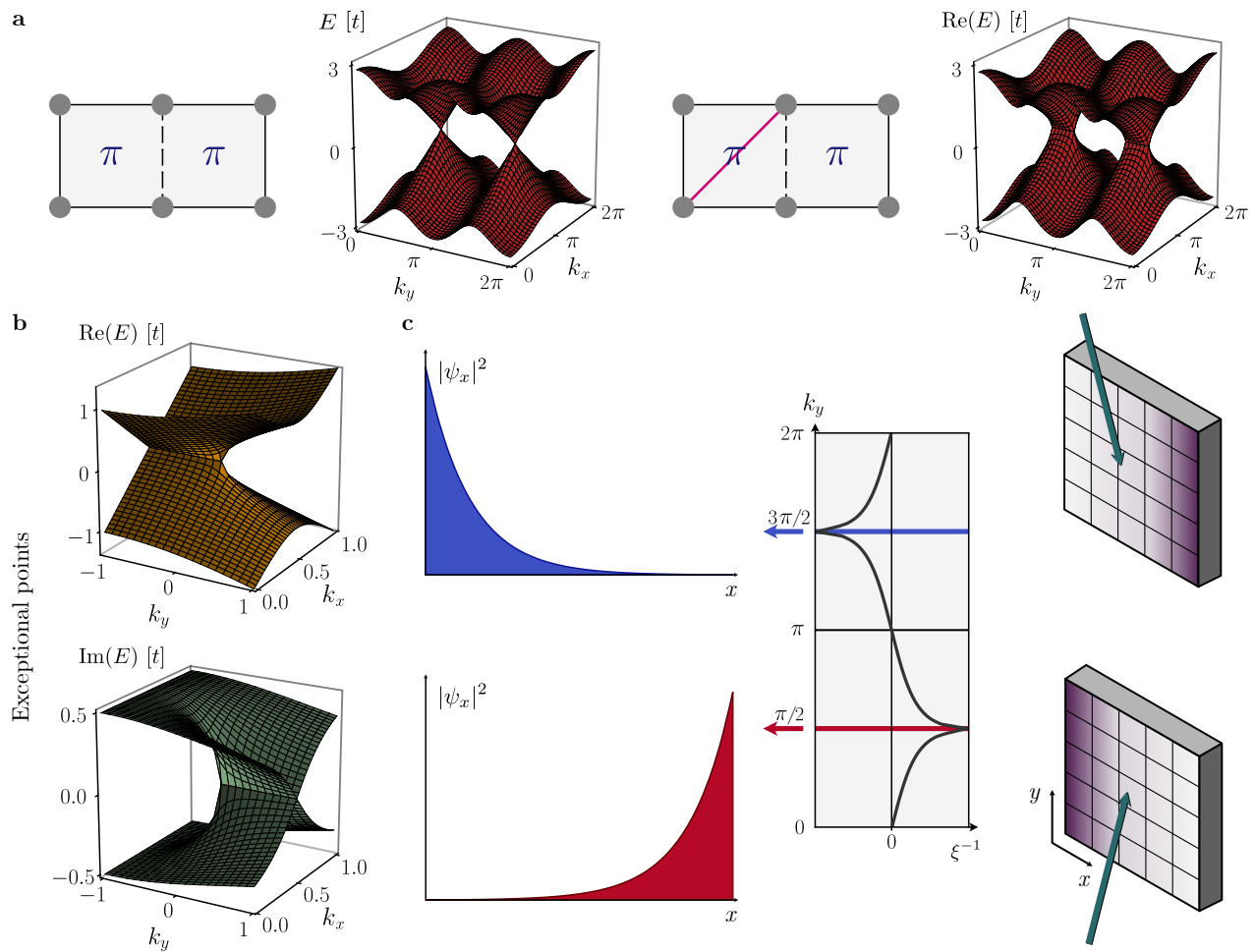


FIG. 1. Theory of the reciprocal skin effect. a) Left: unit cell and spectrum of the π -flux model defined in Eq. (1) with periodic boundary conditions. Solid and dashed lines correspond to hopping amplitudes t and $-t$, respectively. Bands touch in two Dirac points. Right: π -flux model with a non-Hermitian diagonal hopping (pink) included, as defined in Eq. (2). Each Dirac point splits into a pair of exceptional points (only the real part of the band eigenvalues is plotted). b) Real and imaginary part of eigenvalues in the vicinity of an exceptional point, at which two complex eigenvalues are degenerate. c) Schematic of the reciprocal skin effect for OBC in x and PBC in y direction: near two opposite momenta, $k_y = \pi/2$ and $k_y = 3\pi/2$, all eigenstates are exponentially localized with localization length ξ to the left and right of the system, respectively. At $k_y = 0, \pi$ the modes are completely delocalized. Right: The reciprocal skin effect could serve as a direction detector for incident electromagnetic waves: dependent on the propagation direction and polarization, a voltage will build up on the left or right edge of the system, as schematically shown in the figure.

and active circuit elements [34], respectively, while Hermitian hybridization elements relate to inductive and capacitive links between circuit nodes. We design, describe, and measure [39] a non-Hermitian topoelectrical circuit that displays, among exceptional points, the reciprocal skin effect, and is built entirely from capacitors, inductors, and resistors, *without* the need for non-reciprocal active elements such as operational amplifiers. Being a passive circuit network, its convenient translation into alternative platforms of synthetic topological matter promises ubiquitous realization and application in optics, mechanics, and acoustics.

II. THEORY OF THE RECIPROCAL SKIN EFFECT

To underline the generality of our arguments, we will present the theory in the language of (non-Hermitian) tight-binding Hamiltonians, which may represent either a quantum system or the dynamical matrix and response function of a classical system. We start our considerations with the π -flux tight-binding model on a square lattice. It is characterized by a nearest-neighbor hopping t , where exactly one of the four sides of each plaquette has a negative hopping amplitude compared to the three others. These hoppings require a unit cell of two plaquettes of the square lattice [see Fig. 1 a)]. The Bloch Hamiltonian for a system with periodic boundary conditions (PBC) in x and y directions, yielding the momenta k_x and k_y ,

can be written as

$$H_\pi(k_x, k_y) = t \begin{pmatrix} 2 \cos k_y & 1 + e^{-ik_x} \\ 1 + e^{ik_x} & -2 \cos k_y \end{pmatrix}. \quad (1)$$

The model has two Dirac-like band touchings at momenta $(k_x, k_y) = (\pi, \pi/2)$ and $(k_x, k_y) = (\pi, 3\pi/2)$ [see Fig. 1 a) for the band structure].

We add a non-Hermitian (gain/loss) term as a diagonal hopping through one of the plaquettes in the unit cell [see Fig. 1 a)]. It assigns a complex amplitude ir (with r a real number) to the process of a particle hopping along the diagonal toward the upper right, and the exact same amplitude ir to the reversed process. Hermiticity would require that the latter process has the complex conjugated amplitude $-ir$. As such, the addition

$$H(k_x, k_y) = H_\pi(k_x, k_y) - ir \begin{pmatrix} 0 & e^{ik_y} \\ e^{-ik_y} & 0 \end{pmatrix} \quad (2)$$

violates Hermiticity for this diagonal hopping process. Despite its non-Hermiticity, the model still is reciprocal, as it satisfies $H(k_x, k_y) = H^\top(-k_x, -k_y)$ under transposition.

Hamiltonian (2) has two complex-valued eigenbands with remarkable properties: they touch (*i.e.*, the two eigenvalues have equal real and imaginary part) in two pairs of points. Upon introducing a finite r , the Dirac points of the original π -flux model each split into a pair of these points. Such degeneracy points in non-Hermitian systems are called exceptional points and are the generic band touchings in a space with two parameters (here, k_x and k_y). The band structure in the vicinity of an exceptional point is illustrated in Fig. 1 b).

We proceed to consider Hamiltonian (2) with OBC in x -direction, which leaves $k_y \in [0, 2\pi]$ well defined as a boundary momentum, and define $\tilde{H}(k_y)$ as the Hamiltonian for the strip geometry. While $\tilde{H}^\top(k_y) = \tilde{H}(-k_y)$ guarantees reciprocity of the full system, each instance of $\tilde{H}(k_y)$ locally breaks reciprocity for a fixed k_y when seen as a purely one-dimensional model, except for $k_y = -k_y \bmod (2\pi)$. The effective 1D model for a given k_y exhibits the non-Hermitian skin effect as discussed in Refs. 16 and 40: The eigenstates of a Hermitian system form an orthonormal basis whose squared amplitudes, when summed over all states, are equal on all lattice sites. In a non-Hermitian system this need not be the case, since right (left) eigenstates of a non-Hermitian matrix do not individually form an orthonormal basis. As a result, they can all be localized at only one edge of the system, which defines the skin effect. In our model, the skin effect is realized due to the term proportional to r in Eq. (2), which renders the hopping probability for going right different from the probability for going left. This leads to an accumulation of *all eigenstates* towards only one edge.

The *reciprocal skin effect* is characterized by a k_y dependence of this localization property. For $k_y \in (0, \pi)$, all OBC bulk modes localize at the right edge, while the localization switches to the left edge for $k_y \in (\pi, 2\pi)$. The states are delocalized at $k_y = 0, \pi$, because the Hamiltonian $\tilde{H}(k_y)$ is locally reciprocal. We find the strongest localization at $k_y \sim \pi/2, 3\pi/2$, where the initial bulk π -flux model has

its gapless Dirac point. Due to the *global* reciprocity of the Hamiltonian, each localized eigenmode at k_y has a reciprocal partner at $-k_y \bmod 2\pi$, which localizes at the opposing edge.

The reciprocal skin effect in two dimensions is fundamentally different to a doubled and reciprocity-enhanced 1D skin effect, as realized for instance by two reciprocity-reversed Hatano-Nelson chains [41]. To conceptualize this, consider an analogy to the 2D Chern insulator and the 3D Weyl semimetal [42]. Coupling two time-reversed copies of a Chern insulator with chiral edge states constitutes the \mathbb{Z}_2 topological insulator with helical edge states and restores time-reversal symmetry [43]. In a similar fashion, one can create an overall reciprocal system out of two Hatano-Nelson chains, whose exponentially localized modes are not protected by symmetry. Only by the demand of additional symmetries which square to -1 , the precise notion of a \mathbb{Z}_2 skin effect is defined [22]. In distinction to this symmetry enhancement, we consider dimensional enhancement. The Weyl semimetal in 3D can be composed of “slices” of momentum space, which are characterized by a 2D Chern insulator. By analogy, we extend the 1D (non-reciprocal) skin effect to two dimensions, arriving at the reciprocal skin effect, with momentum space slices that host the 1D skin effect. Slices at opposite momenta are connected by the reciprocity transformation. In contrast to one-dimensional systems, hybridization of those reciprocal partners is intrinsically prevented by the translational symmetry of the two-dimensional system.

III. EXPERIMENTAL TOPOLECTRICAL CIRCUIT REALIZATION

In principle, various non-Hermitian, *i.e.*, lossy, classical systems could be deliberately tailored to study the physical effects outlined above. Topoelectrical circuits in particular, however, offer an important advantage due to the only mild limitation imposed by local connectivity constraints otherwise typical to many other metamaterial settings. Most importantly, a connection between the leftmost and rightmost site of a circuit can simply be toggled on/off to change between PBC and OBC. This way, the breakdown of bulk-boundary correspondence can be studied most directly.

We experimentally implemented a circuit which realizes the non-Hermitian but reciprocal model (2) through its response function within linear circuit theory, the circuit Laplacian matrix $J(\omega)$, which takes the role of the reciprocal Hamiltonian previously introduced. It connects the input currents $I_a(\omega)$ at node a of the system to the voltages $V_b(\omega)$ measured at b via Kirchhoff’s law, represented in the frequency domain by $I_a(\omega) = J_{ab}(\omega)V_b(\omega)$. Here we consider a fixed excitation frequency ω , the summation over the repeated index b is implied. (See Supplemental Information for the theory on circuit Laplacians.)

In a Hermitian circuit, all eigenvalues of $J(\omega)$ are purely imaginary [$iJ(\omega)$ is a Hermitian matrix], while the inclusion of resistors generates complex eigenvalues. Interpreting $J(\omega)$ at a fixed frequency ω_0 as a hopping matrix, one observes that

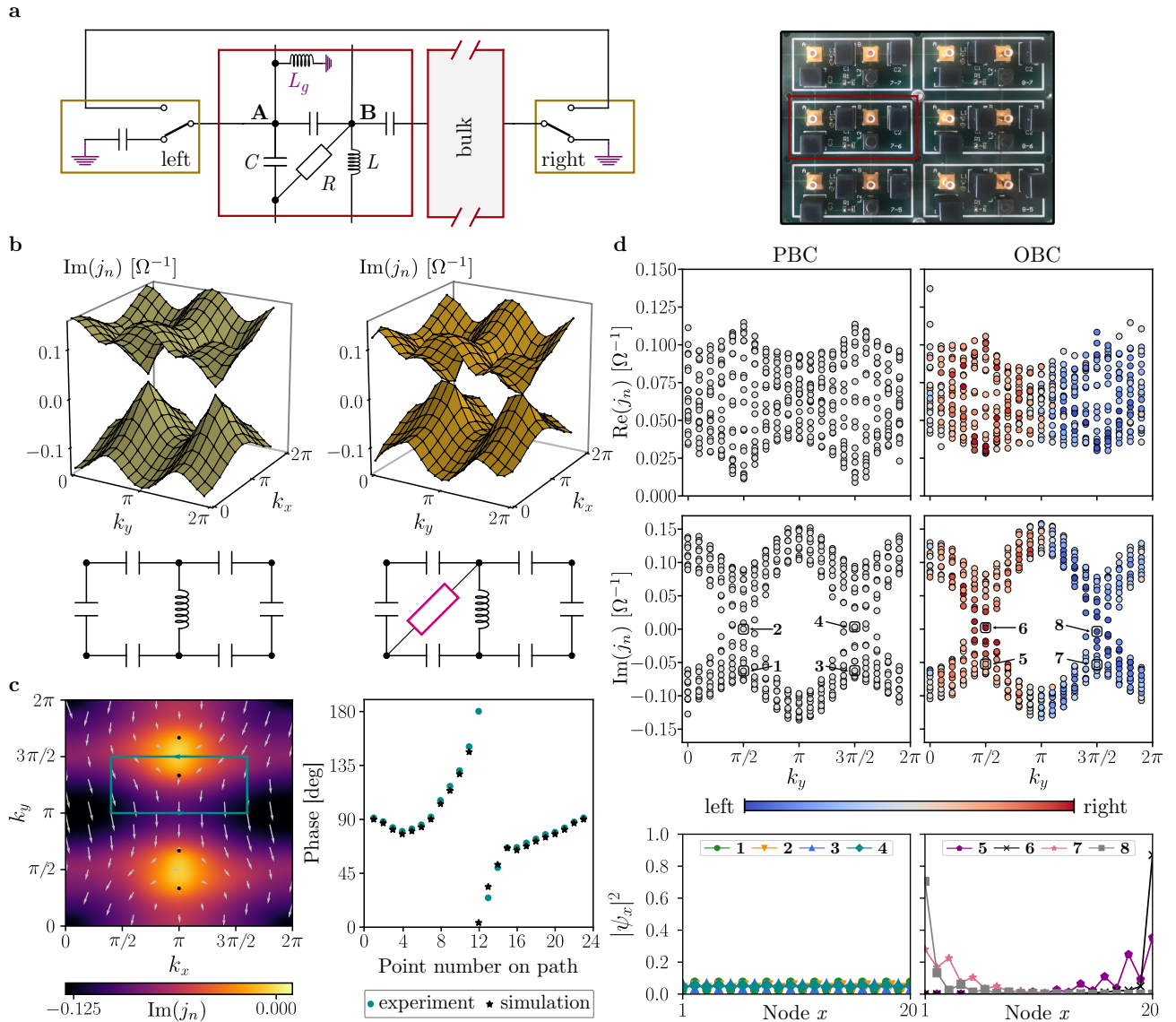


FIG. 2. Experimental topological circuit realization of the reciprocal skin effect and exceptional points. a) Bulk unit cell and boundary terminations of the circuit that realizes the model defined in Eq. (2) and photograph of six unit cells of the assembled circuit board. Appendix C details the connection of this circuit cell to the model in Eq. (2) using the Laplacian formalism. b) Measured spectra with PBCs of the circuit Laplacian and schematic unit cell of the circuit that corresponds to the π -flux model (left) and the non-Hermitian model (right) from Eq. (2) [cf. Fig. 1 a)]. Only the imaginary part of the eigenvalues is plotted. The formation of a branch cut from the Dirac point is visible, the ends of which are host to exceptional points. c) Left: Imaginary part and phase of the eigenvalue along the path indicated is plotted in the right panel. It shows a clear jump by π , indicative of an enclosed exceptional point. (Stars denote a LTSPICE simulation of the circuit, while dots correspond to the measured spectrum.) d) Measured spectra of the circuit Laplacian as a function of k_y for OBC and PBC along the x direction. Localization properties of each eigenstate are indicated by color and determined from the inverse participation ratio (IPR). The bottom panel shows the localization properties of representative individual eigenstates at $k_y = \pi/2$ and $k_y = 3\pi/2$, both for PBC and OBC. The fact that *all* OBC and PBC eigenstates differ non-perturbatively constitutes the reciprocal skin effect, with those around $k_y \sim \pi/2$ right-localized and those around $k_y \sim 3\pi/2$ left-localized.

the sign change of t necessary to implement the π -flux model is achieved by connecting one of the three bonds surrounding a plaquette in a square lattice with an inductor and three with a capacitor [see Fig. 2 a) and b)]. We fabricated a circuit with 10×20 unit cells using this model. (See Supplemental Information for the exact specifications of the circuit.)

Assuming translation invariance (realized to the accuracy of the circuit element specifications), we can represent the voltages and input currents in terms of Fourier modes in reciprocal space. This leads to the k -space representation of the Laplacian as well as its voltage eigenmodes and allows for the definition of a complex-valued admittance band struc-

ture. The latter can be understood as a complex mapping from wave vector k to admittance eigenvalues of the Laplacian. In a measurement, we can decompose the voltage response to an external current excitation and find the eigensystem of the Laplacian for both periodic and open boundary conditions. Figure 2 b) (left) shows the measured bands including the two Dirac-cone band touchings expected for the π -flux model.

Unlike in experimental realizations of the non-reciprocal skin effect [44–46], the reciprocal skin effect can be effected without active elements. For that, we added resistive couplings across the diagonal of every other row of plaquettes, which is analogous to the non-Hermitian term proportional to r in Eq. (2). Figure 2 b) (right) shows the measured bands. The Dirac points are broadened into branch cuts, each of which spans between a pair of exceptional points. To demonstrate this, we plot the phase of the eigenvalue for the band $j_n(\omega_0, k_x, k_y)$ with smaller imaginary part along a closed path in Fig. 2 c). The observed winding and phase jump by π is direct evidence that the path encircles an exceptional point in momentum space, which is topologically stable exactly through this half-integer winding number of the band eigenvalue around it.

Having confirmed that the circuit realizes the desired physics of an exceptional point band structure with PBC, we now present measurements with OBC in x -direction to demonstrate the reciprocal skin effect. Edge terminations are chosen such that the circuit grounding does not introduce undesired off-sets due to a change in the total node conductance at the edge sites, see Fig. 2 a). The measured k_y -resolved spectra are shown in Fig. 2 d), in comparison to an equivalent representation of the data for PBC. The eigenvalues with small imaginary part around $k_y \sim \pi/2, 3\pi/2$ indeed show the expected reorganization from a spectrum with two exceptional points in the bulk towards much fewer states with OBC – a breakdown of the Hermitian bulk-boundary correspondence. The reciprocal skin effect is encoded in the coloring of the data points: red and blue dots correspond to right and left localized eigenstates. (Note that through the measurement of the full matrix $J(\omega_0)$ not only do we have access to its spectrum, but also to all of its eigenstates.) A degree of localization of eigenstates is quantified by the inverse participation ratio (IPR) [47]. Remarkably, *all* states near $k_y \sim \pi/2$ are right-localized, while *all* states near $k_y \sim 3\pi/2$ are left-localized.

IV. DISCUSSION

We have introduced and experimentally demonstrated the concept of a reciprocal skin effect, where the breakdown of bulk-boundary correspondence occurs in the absence of any non-reciprocal coupling. Instead of having extensive mode accumulation all along one boundary, an equal number of eigenmodes localizes along opposite boundaries, with the direction of localization tied to the momentum component parallel to the boundary. Key to their realization is the gain/loss associated with couplings across different sites, which effectively behave like non-reciprocal couplings at a fixed transverse momentum. The reciprocal skin effect can in principle exist in

two or higher dimensions when the non-Hermitian reciprocal couplings connect different internal degrees of freedom and the momentum space structure protects the skin modes from hybridization.

We observed the reciprocal skin effect in an electric circuit with solely passive linear circuit elements. Key to its realization are serial resistors, which are natural candidates for inter-site non-Hermitian loss, instead of active non-reciprocal elements such as operation amplifiers necessary for the non-reciprocal conventional skin effect. The breakdown of bulk-boundary correspondence becomes evident by comparing the PBC system with exceptional points with the markedly different OBC case, featuring oppositely localized skin modes. Our circuit, and more generally the reciprocal skin effect, facilitates novel functionalities when coupled to electromagnetic waves. For instance, it lends itself to potential applications for polarization and direction detectors for electromagnetic waves, where differently directed or polarized input signals are substantially accumulated towards opposite directions.

ACKNOWLEDGMENTS

We thank C. Coulais, S. Huber, V. Vitelli, and Z. Wang for fruitful discussions, as well as M. Hengsberger for guidance with the measurement setup and F. Natterer for lending measurement equipment. The circuit simulations have been performed by the use of LTSPICE. The work in Würzburg is funded by the Deutsche Forschungsgemeinschaft (DFG, German Research Foundation) through project-id 258499086 - SFB 1170 and through the Würzburg-Dresden Cluster of Excellence on Complexity and Topology in Quantum Matter – *ct.qmat* project-id 39085490 - EXC 2147. FS was supported by the Swiss National Science Foundation (grant number: 200021_169061), the National Science Foundation under Grant No. NSF PHY-1748958, and by the Heising-Simons Foundation. MB was supported by the Polish National Agency for Academic Exchange. We further acknowledge support by ERC-StG-Neupert-757867-PARATOP. This research was partially supported under the project STIM – REI, Contract Number: KK.01.1.1.01.0003, a project funded by the European Union through the European Regional Development Fund – the Operational Programme Competitiveness and Cohesion 2014-2020 (KK.01.1.1.01).

Appendix A: Necessary conditions for the reciprocal skin effect

The reciprocal skin effect can occur in any physical system in which reciprocity can be understood as a perfect cancellation of reciprocity-breaking of two oppositely non-reciprocal subsystems. As such, when separated into these subsystems, e.g., specific momentum sectors, a reciprocal system may appear effectively non-reciprocal. While this general observation pertains to most reciprocal systems, we restrict our study to non-Hermitian systems and their individual momentum subsectors, since they allow for the definition of topolog-

ical invariants as key ingredients of bulk-boundary correspondence.

To illustrate the idea, we adopt the language of Hamiltonian matrix elements acting on localized degrees of freedom (nodes). On a finite lattice of at least two dimensions, a coupling λ between two nodes a, b displaced by a distance Y transverse to the boundary gives rise to hopping elements $H_{ab} = \lambda e^{ik_y Y}$ and $H_{ba} = \lambda e^{-ik_y Y}$ in the Hamiltonian matrix by reciprocity defined as $H(k_y) = H^\top(-k_y)$. If λ were real, $H_{ab} = H_{ba}^*$ and the Hamiltonian would not pick up any non-Hermiticity, that is necessary for the skin effect to arise. Suppose λ is complex, *i.e.*, $\lambda = \lambda_0 e^{i\theta}$, where the complex phase θ corresponds to a phase difference of impedance connections in the circuit interpretation. This type of coupling gives rise to a contribution

$$\lambda_0 e^{i\theta} [\cos(k_y Y) \sigma_x + \sin(k_y Y) \sigma_y] \quad (\text{A1})$$

to the Hamiltonian in the (a, b) basis. For $\theta \neq m\pi$, $m \in \mathbb{Z}$, it is manifestly non-Hermitian. By regarding k_y as a parameter and not a variable of the theory, we induce non-reciprocity on individual slices of k_y in the term proportional to σ_y . In particular, the effective non-reciprocity occurs with a nonzero coupling distance Y and its complex-valued prefactor λ . Due to the oddness of $\sin(k_y Y)$ in front of σ_y , states with opposite k_y experience reversed effective non-reciprocity. As a result, these eigenstates at fixed opposite k_y accumulate along opposite boundaries as a consequence of the skin effect.

In common reciprocal system setups such as RLC circuits, this reciprocal skin effect is usually not observed because excitation signals are designed to be almost invariably reciprocal, consisting of an equal superposition of $+k_y$ and $-k_y \bmod 2\pi$ modes. Skin mode accumulation in such systems can however be physically observed, if the input signals are polarized to have unequal $\pm k_y \bmod 2\pi$ weights. This is detailed in methods Sec. F, where differently directed signals, created by suitably designed phase differences between sublattices, are demonstrated to induce voltage responses with a non-reciprocal directional preference.

Appendix B: Non-Hermitian circuit theory

In a passive circuit network of capacitors (C), inductors (L), and resistors (R), currents and voltages are linearly related through a discretized version of the Laplacian operator as a second order spatial derivative. However, energy in such a circuit system is not necessarily conserved, as it can dissipate in an irreversible heating process occurring in resistors. In contrast to purely capacitive or inductive couplings, which oppose the *change* of electric currents or voltages, a resistor opposes the *flow* of an electric current and is, as such, intrinsically non-Hermitian. To be able to analyze the present circuit setup, which involves all of the passive components R, L, C, we rely on non-Hermitian linear circuit theory.

Define V_a and I_a to be the voltage and external input current on node a of a circuit network. Using Kirchhoff's and Ohm's laws, we obtain a coupled system of differential equations for

the circuit,

$$\dot{I}_a = \Gamma_{ab} \ddot{V}_b + \Sigma_{ab} \dot{V}_b + \Lambda_{ab} V_b, \quad (\text{B1})$$

where Γ_{ab} , Σ_{ab} and Λ_{ab} are the reduced Laplacian matrices of capacitances, conductances and inverse inductances, and the summation over repeated indices is implied. The diagonal components $a = b$ of the Laplacians are defined by

$$X_{aa} = -X_{a0} - \sum_{b=1,2,\dots} X_{ab}, \quad X \in \{\Gamma, \Sigma, \Lambda\}, \quad (\text{B2})$$

including the circuit elements X_{a0} between node a and the ground.

A Fourier transformation of Eq. (B1) from the time to frequency domain results in

$$I_a = \left(i\omega \Gamma_{ab} + \Sigma_{ab} - \frac{i}{\omega} \Lambda_{ab} \right) V_b = J_{ab}(\omega) V_b, \quad (\text{B3})$$

where we defined $J_{ab}(\omega)$ as the (grounded) circuit Laplacian [32]. Note that ω is treated as a parameter of the system which is fixed by the external AC driving frequency.

A natural observable in a circuit is the impedance response $Z_{a0}(\omega)$, which is the ratio of the voltage at node a measured with respect to ground due to an input current $I_j = I_0 \delta_{j,a}$ that enters through a and exits through ground. Mathematically, $Z_{a0}(\omega)$ simply involves the inversion of Eq. (B3)

$$\begin{aligned} Z_{a0}(\omega) &= \frac{V_a}{I_0} = \sum_j \frac{G_{aj}(\omega) I_j}{I_0} = G_{aa}(\omega) \\ &= \sum_n \frac{\psi_{n,a} \phi_{n,a}^*}{j_n(\omega)}, \end{aligned} \quad (\text{B4})$$

where $J_{ab}(\omega) = \sum_n j_n(\omega) \psi_{n,a} \phi_{n,b}^*$ defines the spectral representation of the Laplacian with its right and left eigenvectors, ψ_n and ϕ_n . The frequency dependence of the Laplacian eigenvectors remains implicit. As the inverse of the Laplacian, the Green's function $G_{ab}(\omega) = \sum_n j_n^{-1}(\omega) \psi_{n,a} \phi_{n,b}^*$ contains the voltage response to an external current excitation and fundamentally determines both the excitation pattern of individual eigenmodes and the circuit's impedance profile with frequency. The grounding impedances are given by the diagonal elements of G .

The off-diagonal components of the Green's function are accessible using an arrangement of measurements similar to that of the impedance response $Z_{a0}(\omega)$. We feed a current I_a at node a and measure the voltage response $V_b^{(a)}$ at all the other nodes. By repeating this for all input nodes, the Green's function can be reconstructed as

$$G_{ab} = \frac{V_b^{(a)}}{I_a}. \quad (\text{B5})$$

In the circuit formalism, the Green's function as a direct observable contains full information on admittance eigenvalues and eigenmodes of the Laplacian, which can be extracted through numerical diagonalization. The procedure to measure the Green's function can be simplified in periodic models using spatial Fourier transform [39] (see Sec. D).

Appendix C: Theoretical circuit analysis

1. Derivation of the circuit Laplacian

We realize the reciprocal skin effect in an electrical circuit whose unit cell is shown in Fig. 2 a), with the conceptually important elements of each plaquette shown in Fig. 2 b). The two-point Laplacian of a capacitor is given by

$$\begin{pmatrix} I_{\text{in},1} \\ I_{\text{in},2} \end{pmatrix} = i\omega \left[C \begin{pmatrix} 1 & -1 \\ -1 & 1 \end{pmatrix} \right] \begin{pmatrix} V_1 \\ V_2 \end{pmatrix}. \quad (\text{C1})$$

Under omission of the prefactor $i\omega$, the Laplacian matrix is symmetric and Hermitian. The Laplacian for an inductor takes a similar form

$$\begin{pmatrix} I_{\text{in},1} \\ I_{\text{in},2} \end{pmatrix} = i\omega \left[-\frac{1}{\omega^2 L} \begin{pmatrix} 1 & -1 \\ -1 & 1 \end{pmatrix} \right] \begin{pmatrix} V_1 \\ V_2 \end{pmatrix}, \quad (\text{C2})$$

that differs in the frequency-dependent admittance prefactor and, importantly, in the overall sign. At the resonance frequency $\omega_0 = 1/\sqrt{LC}$ of an LC resonator, the inductor effectively acts a negative capacitor, where $-1/(\omega_0^2 L) = -C$ in front of the Laplacian matrix. Therefore, one circuit plaquette of the π -flux model consists of three capacitors (representing t) and an inductor (representing $-t$ at resonance), all of which are Hermitian and reciprocal. At nodes of sublattice A , the diagonal contributions in the Laplacian add to $4C$, whereas for $\omega = \omega_0$ the capacitive and inductive contributions cancel each other in the diagonal term at sublattice B . To avoid the sublattice asymmetry contributing to a σ_z term, we ground nodes of type A with an inductor $L_g \approx L/4$ such that the diagonal contribution to the Laplacian vanishes for both sublattices at resonance frequency. In total, the circuit Laplacian in momentum space is given by

$$J_\pi(k_x, k_y) = i\omega \left[-\begin{pmatrix} 2C \cos(k_y) & C(1 + e^{-ik_x}) \\ C(1 + e^{ik_x}) & 2/(\omega^2 L) \cos(k_y) \end{pmatrix} + \begin{pmatrix} 4C - 1/(\omega^2 L_g) & 0 \\ 0 & 2C - 2/(\omega^2 L) \end{pmatrix} \right] \quad (\text{C3})$$

resembling the π -flux tight-binding model for $\omega \rightarrow \omega_0$, where the second term vanishes.

Additional to $J_\pi(k_x, k_y)$, we introduce a resistor connecting nodes A and B of adjacent unit cells in y -direction [see Fig. 2 a), b)]. Its admittance representation reads

$$\begin{pmatrix} I_{\text{in},1} \\ I_{\text{in},2} \end{pmatrix} = i\omega \left[-\frac{i}{\omega R} \begin{pmatrix} 1 & -e^{ik_y} \\ -e^{-ik_y} & 1 \end{pmatrix} \right] \begin{pmatrix} V_1 \\ V_2 \end{pmatrix} \equiv J_r \begin{pmatrix} V_1 \\ V_2 \end{pmatrix}. \quad (\text{C4})$$

The total Laplacian is given by $J = J_\pi + J_r$. With $i\omega$ factored out, the added Laplacian J_r is non-Hermitian and breaks time-reversal symmetry. For an arbitrary circuit network described by $J(k_x, k_y)$, reciprocity is defined as $J^\top(k_x, k_y) = J(-k_x, -k_y)$. Thus, a resistor is a reciprocal circuit element. However, if one considers a fixed k_y slice of the model, reciprocity is broken as $e^{ik_y} \neq e^{-ik_y}$ for arbitrary $k_y \neq 0, \pi$.

Consider OBC in x -direction, such that the y -direction preserves translational invariance and k_y remains to be well-defined. We find the non-Hermitian skin effect with an extensive number of boundary localized modes, for a range of momenta k_y . The emergence of the skin effect on the level of the tight-binding model is analyzed in the following.

2. Hermitian part of the model

We omit the unit matrix contribution to the circuit Laplacian J and interchangeably consider the tight-binding model that it induces. The Hermitian part of the model is based on the π -flux model with the Hamiltonian

$$H_\pi = [1 + \cos(k_x)] \sigma_x + \sin(k_x) \sigma_y + 2 \cos(k_y) \sigma_z. \quad (\text{C5})$$

It features two Dirac band touchings, which are located on the boundary of the Brillouin zone at $(k_x, k_y) = (\pi, \pi/2), (\pi, 3\pi/2)$. Applying open boundary conditions to the π -flux model in y -direction in a cylindrical geometry results in a pair of counter-propagating modes in the boundary Brillouin zone, as the two Dirac cones are projected onto the same point. There are no topological boundary modes in this configuration. Open boundaries in x -direction preserve the separation of the Dirac crossings at $k_y = \pi/2, 3\pi/2$. If we treat k_y as a parameter instead of as a variable in Eq. (C5), we end up with an effectively one-dimensional hopping model, that is form-invariant to a hopping model on a 1D chain with an additional chiral symmetry breaking mass of $m = 2 \cos(k_y)$ parametrized by k_y . As the amplitudes of the intracell and intercell hoppings of the chain are identical, there will be no topological edge states for open boundary conditions and in particular no flat band joining the two projected Dirac cones in the k_y boundary Brillouin zone.

3. Full non-Hermitian model

We now introduce a non-Hermitian extension to the π -flux model by adding a diagonal coupling across one of the two plaquettes in the unit cell and arrive at the total Hamiltonian

$$H = H_\pi - ir \cos(k_y) \sigma_x + ir \sin(k_y) \sigma_y, \quad (\text{C6})$$

which is related to the circuit Laplacian by $H = [J(\omega_0) - ir\mathbb{1}]/(i\omega_0 C)$ and $r = 1/(\omega_0 RC)$. It is reciprocal, $H(k_x, k_y)^\top = H(-k_x, -k_y)$, in agreement with the fact that it was constructed out of passive elements only. We can tune the strength of the non-Hermiticity by the resistance R , which is chosen such that $r = 1$ in our implementation. The eigenvalues of the Hamiltonian H are complex-valued and the Dirac cones each split into two exceptional points, which are located at $k_x = \pi$ and $k_y = 1/2 \arccos(r^2/2 - 1)$. The exceptional points are band closings of a complex-valued band structure where the corresponding Hamiltonian is defective, *i.e.*, the two eigenvectors coalesce to one and the matrix is a non-diagonalizable Jordan block. The band closing point for k_x remains unchanged upon the added non-Hermiticity.

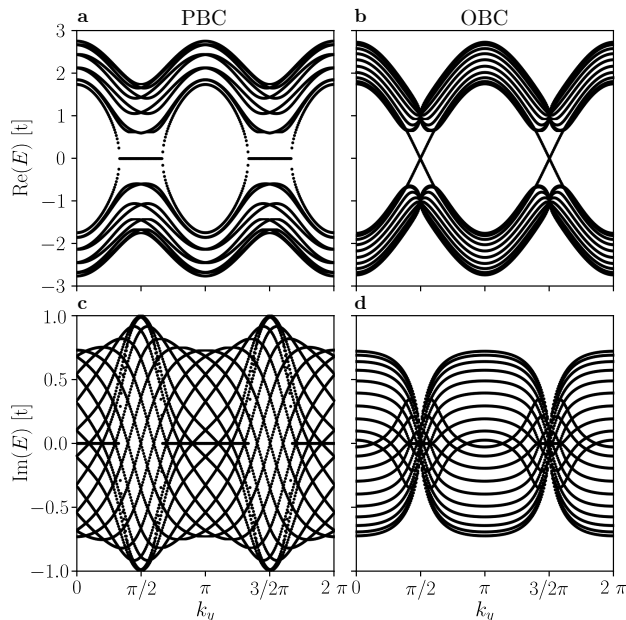


FIG. 3. Numerical calculation of the complex eigenspectrum of the non-Hermitian, non-reciprocal Hamiltonian in eq. (C7) for $r = 1$. (a) Real part of the PBC spectrum, (b) real part of the OBC spectrum, (c) imaginary part of the PBC spectrum, (d) imaginary part of the OBC spectrum. There is a non-trivial spectral flow from PBC to OBC, which manifests the breakdown of bulk-boundary correspondence associated with the extensive localization of eigenmodes.

For $r = 1$, the four PBC exceptional points are pinned to $k_y = \pm\pi/3, \pm 2\pi/3 \pmod{2\pi}$.

The effectively one-dimensional model obtained by treating k_y as a parameter is extended by two non-Hermitian terms resulting in

$$H_{k_y}(k_x) = [1 + \cos(k_x) - ir_x] \sigma_x + [\sin(k_x) + ir_y] \sigma_y + m \sigma_z \quad (\text{C7})$$

with $r_x = r \cos(k_y)$, $r_y = r \sin(k_y)$ and $m = 2 \cos(k_y)$. The spectrum of $H_{k_y}(k_x)$ for periodic and open boundary conditions is shown in Fig. 3 for $r = 1$. The spectra for OBC and PBC are manifestly different demonstrating the non-trivial spectral flow.

If we fix k_y to one particular value, which means taking r_x , r_y and m as constants, $H_{k_y}(k_x)$ breaks reciprocity resulting from the term $ir_y \sigma_y$. The combined breaking of reciprocity and Hermiticity in this model gives rise to the one-dimensional skin effect for $r_y \neq 0$ [16, 17, 19].

The bulk modes of the OBC Hamiltonian are localized on one boundary of the system with $\psi_x \sim e^{-x/\xi}$, where

$$\begin{aligned} \xi^{-1} &= \frac{1}{4} \ln \left(\frac{(1+r_y)^2 + r_x^2}{(1-r_y)^2 + r_x^2} \right) \\ &= \frac{1}{4} \ln \left(\frac{1+r^2 + 2r \sin(k_y)}{1+r^2 - 2r \sin(k_y)} \right). \end{aligned} \quad (\text{C8})$$

The localization length ξ is positive, if $k_y \in (0, \pi)$ and negative if $k_y \in (\pi, 2\pi)$ in the boundary Brillouin zone with open boundaries along x . This leads to left edge localized modes, if $k_y \in (0, \pi)$ and to right edge localization, if $k_y \in (\pi, 2\pi)$. The strongest localization is found at the original positions of the Dirac crossings in the boundary Brillouin zone, $k_y = \pi/2, 3\pi/2$. At those points, ξ vanishes for $r \rightarrow 1$ leading to infinite localization, which is accompanied by exceptional points in the OBC spectrum of the model. The localization inherits a reciprocal symmetry from the full model as $\xi(-k_y) = -\xi(k_y)$. A state at k_y has a reciprocal partner mode at $-k_y \pmod{2\pi}$, which possesses the same absolute localization length, but is localized on the opposite edge. Combining those partners preserves reciprocity in the full model. For $k_y = 0$ or π , the localization length diverges. The corresponding bulk eigenstates are delocalized and bulk-boundary correspondence is restored. This roots in the fact that $r_y = 0$ at $k_y = 0$ or π and $H_{0,\pi}(k_x)$ is reciprocal leading to a matching of the PBC and OBC spectrum.

Due to the inclusion of non-Hermitian terms, topological states can emerge in the full Hamiltonian, that have not been present in the initial Hermitian π -flux model. Our discussion closely follows Ref. 16. To study the topological aspects in the system with N unit cells, we perform a *non-unitary* transformation $H'_{k_y} = S^{-1} H_{k_y} S$ with $S = \text{diag}(1, a, a, a^2, a^2, \dots, a^{N-1}, a^N)$ and $a = \sqrt{(1-ir_x - r_y)/(1-ir_x + r_y)}$, where open boundary conditions are implied. The transformed Hamiltonian under application of PBCs can be rewritten as a reciprocal Su-Schrieffer-Heeger (SSH) chain with complex coefficients,

$$H'_{k_y} = [t_0 + \cos(k_x)] \sigma_x + [\sin(k_x)] \sigma_y + m \sigma_z, \quad (\text{C9})$$

where $t_0 = \sqrt{(1-ir_x)^2 - r_y^2} \in \mathbb{C}$. SSH-type edge modes exist on both edges of the system, if $|t_0| < 1$, which translates to a topological regime for

$$\cos(k_y) < \sqrt{\frac{1}{2} - \left(\frac{r}{2}\right)^2}, \quad (\text{C10})$$

parametrized by the momentum k_y . The bulk spectrum of H'_{k_y} is gapped, if either $t_0 \neq 1$ or $m \neq 0$. The gap closes at $r = \sqrt{2}$ for $k_y = \pi/2$, which marks the topological phase transition in r . If $r \geq \sqrt{2}$, there are no topological states. As the spectra of H'_{k_y} and H_{k_y} are identical, the total Hamiltonian with OBCs in x -direction exhibits a bulk gap for all k_y in the boundary Brillouin zone for $r \neq \sqrt{2}$. The topological phase transition does in general not occur at the PBC band closings, but is instead parametrically displaced due to the non-Hermiticity. Only for the special choice of $r = 1$, the two conditions coincide, resulting in topological transitions at the PBC exceptional points for $k_y = \pm\pi/3, \pm 2\pi/3 \pmod{2\pi}$. The topological boundary modes disperse with $\pm m = \pm 2 \cos(k_y)$ and assume a linear dispersion at the original location of the Dirac crossings in the non-Hermitian model at $k_y = \pi/2, 3\pi/2$ in the boundary Brillouin zone. Note that the bulk is gapped at those points, while the edge

states cross at zero energy. The analysis shows that SSH-type modes can coexist with skin modes in the non-Hermitian model with open boundaries along x .

Appendix D: Experimental circuit implementation

The circuit board was fitted with metallized polypropylene film capacitors (Vishay MKP1837410161G, 100nF 160V) implementing C and SMD power inductors of $33\mu\text{H}$ (Bourns SRR0604-330KL, max. $250\text{m}\Omega$ DC resistance) for L and $8.2\mu\text{H}$ (TDK MLF2012E8R2JT000, max. $700\text{m}\Omega$ DC resistance) for L_g . For R we use the 18Ω resistor (Yageo RC1206FR-0718RL). The capacitors and resistors have a tolerance of 1% and were therefore not characterized. All inductances were pre-characterized with the Hameg HM8118 LCR Brige to obtain tolerances of below 1% of the nominal component values.

The measurement was conducted at the frequency of 87.25 kHz, which was identified as the resonance frequency $f_0 = \omega_0/(2\pi)$. This frequency differs from the nominal value of $1/\sqrt{LC}$ as parasitic effects in the inductors and capacitors shift the resonance. To find the measurement frequency, a frequency sweep of the voltage at a node A and a node B due to a current excitation was done and compared to an LTSPICE simulation of the circuit including parasitic resistances. On the basis of features such as local minima and maxima in the frequency sweep the resonance frequency could be identified.

The circuit was fed by the sine wave generator of a lock-in amplifier (Zurich Instruments MFLI series). We worked with an input signal with an amplitude of 900 mV. The current was measured with an Oscilloscope (Rhode & Schwarz RTM 1054) over a resistor (11Ω). In order to measure the band structure of the circuit, we fed the current into a node via the resistor and we measured the voltage response due to the excitation at all nodes. For the voltage measurements, the same lock-in amplifier was used. We perform a Fourier transformation of the input current and voltage vector, for PBC in x and y direction and for OBC in y direction only. Using Eq. (B5), we can reconstruct one column of the Green's function for all wave vectors. By repeating this procedure for all other *inequivalent* nodes, the complete Green's function is accessible. For PBC only the different nodes in the unit cell are inequivalent, whereas for OBC all nodes in the non-periodic direction serve as current input for a set of measurements. After the Green's function is determined, we obtain the eigenvalues and eigenvectors by diagonalizing it. For details on the measurement process see Ref. 39.

Appendix E: Representation of the Laplacian spectra in the complex plane

We present an alternative representation of the complex spectra of the circuit Laplacian, both theoretical and experimental. For this, we consider k_y as a parameter and plot for each fixed k_y the set of eigenvalues in the complex plane

$\text{Re}(j_n)$ - $\text{Im}(j_n)$. This generates a two-dimensional closed surface, as shown in Fig. 4 a) for PBC. As a function of k_y , the eigenvalues trace out either a single circle or two circles in the $\text{Re}(j_n)$ - $\text{Im}(j_n)$ plane. The transitions between these two topologically distinct situations are exceptional points. The planes $k_y = 0$ and $k_y = \pi$ are special, because the path traced out in the complex plane as a function of k_x is reciprocal on them. Therefore, it collapses into lines on which each non-end point is visited two times as k_x is varied[19].

In summary, since we have two pairs of exceptional points, the two-dimensional eigenvalue surface in k_y - $\text{Re}(j_n)$ - $\text{Im}(j_n)$ space has genus three[48]. We can plot the experimental spectra of $J(\omega_0)$ in a similar fashion, shown in Fig. 4 c). We observe, for PBC, a clear from slices at constant k_y with a single circle and two circles in the complex plane of eigenvalues. This strongly indicates the presence of exceptional points between these two slices.

Appendix F: Response of the reciprocal skin-effect circuit to bulk perturbations

A distinct feature of the reciprocal skin effect, which may lead to applications for polarization detection of electromagnetic waves, is the response to the circuit to perturbations in the bulk. From Eq. (B3) we deduce that the voltage response at site a to a driving current at frequency ω is given by

$$V_a = J_{ab}^{-1}(\omega)I_b. \quad (\text{F1})$$

Since our circuit has finite resistivity, $J_{ab}(\omega)$ has no zero eigenvalues at real frequencies, and can therefore be readily inverted. To model the experimental situation, we consider PBC in y -direction and OBC in x -direction. We then apply a minimal driving current to two bulk sites aligned along the y -direction, where we assign the current at one site a $+\pi/2$ ($-\pi/2$) phase shift with respect to the current at the other site. We therefore expect the current to excite the circuit Laplacian eigenstates at $k_y = \pi/2$ ($k_y = 3\pi/2$), which are right (left) localized in x -direction due to the reciprocal skin effect. Figure 5 shows the theoretically calculated response of the circuit that is obtained by inverting the real-space version of the Hamiltonian given by Eq. (2). We find that the two driving current patterns indeed lead to nonlocal voltage responses at the far right (left) of the circuit. The reciprocal skin effect could therefore be the basis of a polarization detection device for electromagnetic radiation.

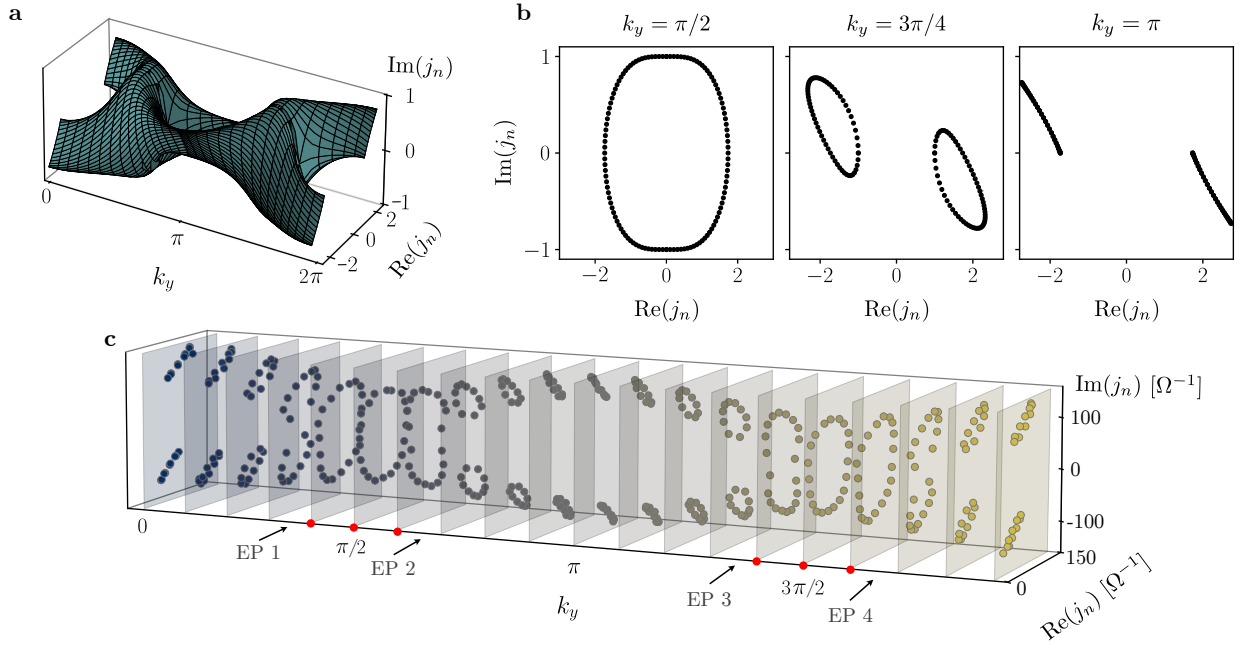


FIG. 4. Representation of the circuit Laplacian spectra for periodic boundary conditions (PBC) in the complex plane as a function of k_y . a) Theoretically computed spectrum showing a genus three surface with four exceptional points. b) Slice plots obtained from a) for three different k_y . c) Measured spectra, where each of the four transitions from a single circle in the complex plane to two circles marks an exceptional point (EP1–EP4) as a function of k_y .

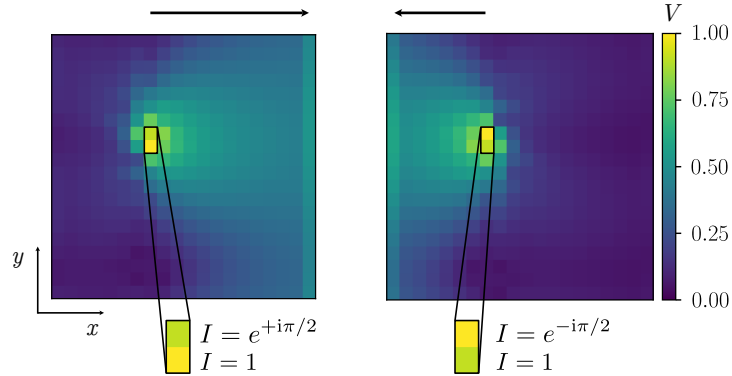


FIG. 5. Reciprocal skin effect voltage response due to a localized bulk driving current with phase shift. The sites where the current is applied are framed in black, the zoom-ins show how the relative phase is implemented. Importantly, for a phase shift of $+\pi/2$ ($-\pi/2$) we find a nonlocal voltage response at the far right (left) side of the circuit with OBC, which is absent for phase shifts 0 and π . The arrows show the direction of voltage accumulation.

- [1] F. Bloch, Über die Quantenmechanik der Elektronen in Kristallgittern, *Zeitschrift für Physik* **52**, 555 (1929).
- [2] K. v. Klitzing, G. Dorda, and M. Pepper, New method for high-accuracy determination of the fine-structure constant based on quantized hall resistance, *Phys. Rev. Lett.* **45**, 494 (1980).
- [3] F. D. M. Haldane, Model for a quantum hall effect without landau levels: Condensed-matter realization of the "parity anomaly", *Physical Review Letters* **61**, 2015 (1988).
- [4] M. König, S. Wiedmann, C. Brüne, A. Roth, H. Buhmann, L. W. Molenkamp, X.-L. Qi, and S.-C. Zhang, Quantum spin hall insulator state in hgte quantum wells, *Science* **318**, 766 (2007).
- [5] X.-L. Qi and S.-C. Zhang, Topological insulators and superconductors, *Rev. Mod. Phys.* **83**, 1057 (2011).
- [6] M. Z. Hasan and C. L. Kane, Colloquium: Topological insulators, *Rev. Mod. Phys.* **82**, 3045 (2010).
- [7] N. P. Armitage, E. J. Mele, and A. Vishwanath, Weyl and dirac semimetals in three-dimensional solids, *Rev. Mod. Phys.* **90**, 015001 (2018).
- [8] Y. Hatsugai, Chern number and edge states in the integer quantum hall effect, *Phys. Rev. Lett.* **71**, 3697 (1993).
- [9] E. Prodan and H. Schulz-Baldes, *Bulk and boundary invariants for complex topological insulators* (Springer).
- [10] Z. Gong, Y. Ashida, K. Kawabata, K. Takasan, S. Higashikawa, and M. Ueda, Topological phases of non-hermitian systems, *Phys. Rev. X* **8**, 031079 (2018).
- [11] L. E. F. Foa Torres, Perspective on topological states of non-hermitian lattices, *Journal of Physics: Materials* (2019).
- [12] T. E. Lee, Anomalous edge state in a non-hermitian lattice, *Phys. Rev. Lett.* **116**, 133903 (2016).
- [13] V. M. Martinez Alvarez, J. E. Barrios Vargas, and L. E. F. Foa Torres, Non-hermitian robust edge states in one dimension: Anomalous localization and eigenspace condensation at exceptional points, *Phys. Rev. B* **97**, 121401 (2018).
- [14] H. Shen, B. Zhen, and L. Fu, Topological band theory for non-hermitian hamiltonians, *Phys. Rev. Lett.* **120**, 146402 (2018).
- [15] H. Zhou, C. Peng, Y. Yoon, C. W. Hsu, K. A. Nelson, L. Fu, J. D. Joannopoulos, M. Soljačić, and B. Zhen, Observation of bulk fermi arc and polarization half charge from paired exceptional points, *Science* **359**, 1009 (2018).
- [16] S. Yao and Z. Wang, Edge states and topological invariants of non-hermitian systems, *Phys. Rev. Lett.* **121**, 086803 (2018).
- [17] Y. Xiong, Why does bulk boundary correspondence fail in some non-hermitian topological models, *Journal of Physics Communications* **2**, 035043 (2018).
- [18] F. K. Kunst, E. Edvardsson, J. C. Budich, and E. J. Bergholtz, Biorthogonal bulk-boundary correspondence in non-hermitian systems, *Phys. Rev. Lett.* **121**, 026808 (2018).
- [19] C. H. Lee and R. Thomale, Anatomy of skin modes and topology in non-hermitian systems, *Phys. Rev. B* **99**, 201103 (2019).
- [20] D. S. Borgnia, A. Jura Kruchkov, and R.-J. Slager, Non-Hermitian Boundary Modes, arXiv e-prints, arXiv:1902.07217 (2019), arXiv:1902.07217 [cond-mat.mes-hall].
- [21] W. B. Rui, M. M. Hirschmann, and A. P. Schnyder, Ptsymmetric non-hermitian dirac semimetals, *Phys. Rev. B* **100**, 245116 (2019).
- [22] N. Okuma, K. Kawabata, K. Shiozaki, and M. Sato, Topological origin of non-hermitian skin effects (2019), arXiv:1910.02878 [cond-mat.mes-hall].
- [23] M. V. Berry, Quantal phase factors accompanying adiabatic changes, *Proceedings of the Royal Society of London A: Mathematical, Physical and Engineering Sciences* **392**, 45 (1984).
- [24] J. Zak, Berry's phase for energy bands in solids, *Phys. Rev. Lett.* **62**, 2747 (1989).
- [25] F. D. M. Haldane, Path dependence of the geometric rotation of polarization in optical fibers, *Opt. Lett.* **11**, 730 (1986).
- [26] F. D. M. Haldane and S. Raghu, Possible realization of directional optical waveguides in photonic crystals with broken time-reversal symmetry, *Phys. Rev. Lett.* **100**, 013904 (2008).
- [27] C. L. Kane and T. C. Lubensky, Topological boundary modes in isostatic lattices, *Nat Phys* **10**, 39 (2014).
- [28] Z. Yang, F. Gao, X. Shi, X. Lin, Z. Gao, Y. Chong, and B. Zhang, Topological acoustics, *Phys. Rev. Lett.* **114**, 114301 (2015).
- [29] J. Ningyuan, C. Owens, A. Sommer, D. Schuster, and J. Simon, Time- and site-resolved dynamics in a topological circuit, *Phys. Rev. X* **5**, 021031 (2015).
- [30] V. V. Albert, L. I. Glazman, and L. Jiang, Topological properties of linear circuit lattices, *Phys. Rev. Lett.* **114**, 173902 (2015).
- [31] W. Hu, J. C. Pillay, K. Wu, M. Pasek, P. P. Shum, and Y. Chong, Measurement of a topological edge invariant in a microwave network, *Physical Review X* **5**, 011012 (2015).
- [32] C. H. Lee, S. Imhof, C. Berger, F. Bayer, J. Brehm, L. W. Molenkamp, T. Kiessling, and R. Thomale, Topoelectrical circuits, *Communications Physics* **1**, 39 (2018).
- [33] S. Imhof, C. Berger, F. Bayer, J. Brehm, L. W. Molenkamp, T. Kiessling, F. Schindler, C. H. Lee, M. Greiter, T. Neupert, and R. Thomale, Topoelectrical-circuit realization of topological corner modes, *Nature Physics* **14**, 925 (2018).
- [34] T. Hofmann, T. Helbig, C. H. Lee, M. Greiter, and R. Thomale, Chiral voltage propagation and calibration in a topoelectrical chern circuit, *Phys. Rev. Lett.* **122**, 247702 (2019).
- [35] C. H. Lee, T. Hofmann, T. Helbig, Y. Liu, X. Zhang, M. Greiter, and R. Thomale, Imaging nodal knots in momentum space through topoelectrical circuits, arXiv:1904.10183.
- [36] M. Ezawa, Non-hermitian boundary and interface states in non-reciprocal higher-order topological metals and electrical circuits, *Phys. Rev. B* **99**, 121411 (2019).
- [37] M. Ezawa, Electric circuits for non-Hermitian Chern insulators, arXiv e-prints, arXiv:1904.03823 (2019), arXiv:1904.03823 [cond-mat.mes-hall].
- [38] Y. Wang, L.-J. Lang, C. H. Lee, B. Zhang, and Y. Chong, Topologically enhanced harmonic generation in a nonlinear transmission line metamaterial, *Nature communications* **10**, 1102 (2019).
- [39] T. Helbig, T. Hofmann, C. H. Lee, R. Thomale, S. Imhof, L. W. Molenkamp, and T. Kiessling, Band structure engineering and reconstruction in electric circuit networks, *Phys. Rev. B* **99**, 161114 (2019).
- [40] F. Song, S. Yao, and Z. Wang, Non-hermitian skin effect and chiral damping in open quantum systems, arXiv preprint arXiv:1904.08432 (2019).
- [41] N. Hatano and D. R. Nelson, Localization transitions in non-hermitian quantum mechanics, *Phys. Rev. Lett.* **77**, 570 (1996).
- [42] S. Murakami, Phase transition between the quantum spin hall and insulator phases in 3d: emergence of a topological gapless phase, *New Journal of Physics* **9**, 356 (2007).
- [43] C. L. Kane and E. J. Mele, Z_2 , *Phys. Rev. Lett.* **95**, 146802 (2005).
- [44] T. Helbig, T. Hofmann, S. Imhof, M. Abdelghany, T. Kiessling, L. W. Molenkamp, C. H. Lee, A. Szameit, M. Greiter, and R. Thomale, Observation of bulk boundary correspon-

- dence breakdown in topoelectrical circuits, arXiv e-prints , arXiv:1907.11562 (2019), arXiv:1907.11562 [cond-mat.mes-hall].
- [45] A. Ghatak, M. Brandenbourger, J. van Wezel, and C. Coulais, Observation of non-Hermitian topology and its bulk-edge correspondence, arXiv e-prints , arXiv:1907.11619 (2019), arXiv:1907.11619 [cond-mat.mes-hall].
- [46] L. Xiao, T. Deng, K. Wang, G. Zhu, Z. Wang, W. Yi, and P. Xue, Observation of non-Hermitian bulk-boundary correspondence in quantum dynamics, arXiv e-prints , arXiv:1907.12566 (2019), arXiv:1907.12566 [cond-mat.mes-hall].
- [47] F. Evers and A. D. Mirlin, Anderson transitions, *Rev. Mod. Phys.* **80**, 1355 (2008).
- [48] C. H. Lee, G. Li, Y. Liu, T. Tai, R. Thomale, and X. Zhang, Tidal surface states as fingerprints of non-hermitian nodal knot metals, arXiv preprint arXiv:1812.02011 (2018).